C. R. Mecanique 340 (2012) 882–893

Contents lists available at SciVerse ScienceDirect

Comptes Rendus Mecanique

www.sciencedirect.com

Out of Equilibrium Dynamics

Ignition time of hydrogen–air diffusion flames

Antonio L. Sánchez [a,b,*], Eduardo Fernández-Tarrazo [b], Pierre Boivin [b], Amable Liñán [c], Forman A. Williams [a]

[a] Department of Mechanical and Aerospace Engineering, University of California, San Diego, La Jolla, CA 92093-0411, USA
[b] Grupo de Mecánica de Fluidos, Universidad Carlos III de Madrid, 28911 Leganés, Spain
[c] ETSI Aeronáuticos, Universidad Politécnica de Madrid, 28040 Madrid, Spain

ARTICLE INFO

Article history:
Available online 13 November 2012

Keywords:
Hydrogen ignition
Supersonic combustion
SCRAMJETS

ABSTRACT

The ignition time of hydrogen–air diffusion flames is a quantity of utmost interest in a large number of applications, with implications regarding the viability of supersonic combustion and the safe operation of gas turbines. The underlying chemistry and the associated ignition history are very different depending on the initial temperature and pressure. This article addresses conditions that place the system above the so-called second explosion limit, as is typically the case in SCRAMJET operation, so that a branched-chain explosion characterizes the ignition process. The roles of local radical accumulation, molecular transport, and chemical reaction in nonpremixed ignition are clarified by considering the temporal evolution of an unstrained mixing layer formed between two semi-infinite spaces of hydrogen and air. The problem is formulated in terms of a radical-pool mass fraction, whose evolution in time is studied with a WKB expansion that exploits the disparity of chemical time scales present in the problem, leading to an explicit expression for the ignition time. The applicability of the analytical results for obtaining predictions of ignition distances in supersonic-combustion applications is also considered.

1. Introduction

In nonpremixed combustion devices the air and the fuel mix and react after entering the combustion chamber through separate feed streams. For the high Reynolds numbers typically encountered in practical burners the flow is turbulent. Molecular mixing and chemical reaction occur at the interface between the reactant streams in thin mixing layers strained by the outer flow [1]. When the flow velocity is sufficiently large, as occurs in supersonic-combustion applications, no upstream flame propagation is possible, and combustion stabilization relies on autoignition of the mixture [2]. The combustion zone appears downstream from the injection point at a distance such that the mixture, convected downstream with the mean flow, has had sufficient time to self-ignite. The effect of flow stretch tends to delay ignition, as first noticed by Niioka [3], so that autoignition is seen to occur in regions of low scalar dissipation, as revealed by numerical and experimental studies [4].

The character of the autoignition process depends on the chemistry of the specific fuel considered. A thermal explosion, including a sudden thermal runaway at a well-defined time, appears often when the controlling chemical reaction has a high temperature sensitivity. The associated mixing-layer ignition problem was investigated by Liñán and Crespo [5] with a 1-step irreversible Arrhenius reaction adopted for the chemistry description, an analysis that was later extended by Niioka [3]

* Corresponding author at: Grupo de Mecánica de Fluidos, Universidad Carlos III de Madrid, 28911 Leganés, Spain.
E-mail addresses: asanchez@ing.uc3m.es (A.L. Sánchez), eafernan@ing.uc3m.es (E. Fernández-Tarrazo), pierre.boivin@polytechnique.edu (P. Boivin), amable.linan@upm.es (A. Liñán), faw@ucsd.edu (F.A. Williams).

1631-0721/$ – see front matter
http://dx.doi.org/10.1016/j.crme.2012.10.035

Table 1
The 5-step mechanism for hydrogen–air high-temperature ignition with rate coefficients in Arrhenius form $k = AT^n \exp(-E/R^0T)$.

	Reaction		A[a]	n	E[a]
1	$H + O_2 \rightarrow OH + O$	k_1	3.52×10^{16}	−0.7	71.42
2	$H_2 + O \rightarrow OH + H$	k_2	5.06×10^{4}	2.67	26.32
3	$H_2 + OH \rightarrow H_2O + H$	k_3	1.17×10^{9}	1.3	15.21
4	$H + O_2 + M \rightarrow HO_2 + M$[b]	k_0	5.75×10^{19}	−1.4	0.0
		k_∞	4.65×10^{12}	0.44	0.0
5	$H_2 + O_2 \rightarrow HO_2 + H$	k_5	2.69×10^{12}	0.36	231.86

[a] Units are mol, s, cm^3, kJ, and K.
[b] Chaperon efficiencies are 2.5 for H_2, 16.0 for H_2O, and 1.0 for all other species; Troe falloff with $F_c = 0.5$.

to account for the effect of flow strain. By way of contrast, for hydrogen or for fuel mixtures containing a significant amount of hydrogen (e.g., syngas mixtures), a branched-chain explosion with quasi-isothermal autocatalytic radical growth characterizes the ignition process when the feed-stream temperature is above the so-called crossover temperature [6], the conditions of interest for SCRAMJET operation.[1]

The problem of hydrogen–air autoignition in SCRAMJET-like configurations has been considered previously in numerous papers [4], a recent example being the study of Boivin et at. [8] (see also [9]), whose results were validated by comparison with the experimental measurements of Cheng et al. [10]. Due to the complexity of the resulting flow, it is rather difficult to extract information from the numerics on the role of the different physicochemical mechanisms involved in the ignition process. To that end, theoretical analyses of hydrogen–air mixing-layer ignition incorporating realistic chemistry are often more useful (see, e.g., [11–13]), in that they serve to clarify more readily the underlying competing phenomena, that being the purpose of the present paper.

As a simplified case, we neglect herein the effect of flow strain on the ignition process, and focus instead on the time evolution of the unstrained mixing layer formed between two semi-infinite spaces of hydrogen and air. Unlike previous mixing-layer theoretical studies [11–13], full account is taken of variations of density and transport properties with temperature and molecular mass, and an explicit analytical solution is presented for the mixing process in isothermal hydrogen–air mixing layers. We shall see how the starting chemistry, including five elementary reactions with H, O and OH as chemical intermediates, can be conveniently simplified by introducing a radical-pool variable that appropriately accounts for the departures from steady state of O and OH, thereby reducing the description of the branched-chain explosion to the integration of a single evolution equation. An asymptotic analysis based on the disparity of time scales involved in the problem will be performed, showing how the effects of transverse mixing and radical loss by diffusion influence the ignition history. Also, the development leads to a simple explicit expression for the ignition time. We shall show how the product of this ignition time and the average convection velocity may be used to provide a simple estimate for the ignition distance in SCRAMJET devices.

We begin the presentation in Section 2 by using the case of homogeneous ignition as an example to discuss various simplifications to the chemistry, to be used later in the mixing-layer problem, which is next formulated in Section 3. The asymptotic analysis is presented in Section 4, followed by some concluding remarks in Section 5.

2. Simplifications to the chemistry description

2.1. Hydrogen–air ignition chemistry

Although detailed chemical-kinetic mechanisms for hydrogen–air combustion, such as the so-called San Diego Mechanism [14], include up to 21 reversible elementary reactions, description of the branched-chain explosion leading to ignition in high-temperature environments requires only consideration of the five elementary reactions shown in Table 1. Since radical concentrations are low prior to ignition, radical regeneration through HO_2 attack by H and OH is typically unimportant and has been correspondingly neglected in writing the short mechanism, thereby causing HO_2 to behave effectively as a product in the 5-step chemistry description. Radical buildup during ignition depends on the competition of the shuffle reactions 1–3 with the recombination reaction 4, with the former being progressively more dominant as the temperature increases above the so-called crossover temperature, defined below in (7). Although the reaction-rate constant of reaction 5 is much smaller than those of the other reactions in the temperature range of interest, so that for instance $k_5/k_1 \simeq 1.45 \times 10^{-8}$ at $T = 1200$ K, this reaction must be included in the mechanism to provide the initial radical growth when radicals are absent at the initial instant.

The accuracy with which the 5-step mechanism reproduces the detailed-chemistry results is illustrated in Fig. 1, which shows the evolution with time of the temperature and of the mole fractions X_H and X_{H_2} in a stoichiometric H_2–air mixture contained in a homogeneous adiabatic reactor at constant atmospheric pressure $p = 1$ atm and with initial temperature

[1] It is of interest to note that, as revealed in recent work [7], a thermal explosion characterizes hydrogen ignition for conditions below crossover, found for instance in gas-turbine mixers upstream from the combustion chamber, so that the corresponding mixing-layer ignition would be similar to that described by Liñán and Crespo [5].

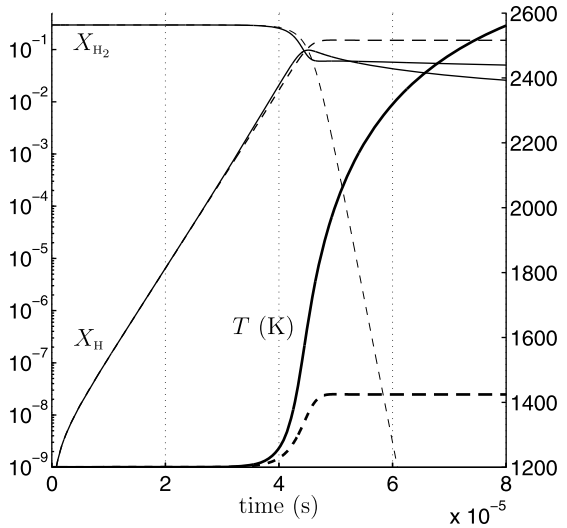

Fig. 1. The time evolution of X_{H_2}, X_H, and T for a stoichiometric hydrogen–air mixture in a homogeneous adiabatic reactor at constant atmospheric pressure and initial temperature $T = 1200$ K as obtained from numerical integrations with the SD mechanism (solid curves) and with the 5-step mechanism (dashed curves).

$T = 1200$ K. As can be seen, the reaction history includes an induction stage of exponential radical growth with negligible reactant consumption and negligible heat release, followed by a stage of radical recombination with progressive temperature increase. It can be seen in the plot that the 5-step mechanism describes accurately the radical growth during the branched-chain explosion until the peak radical concentration is reached. Ignition times can be identified with the temperature-inflection criterion or with the occurrence of a maximum in the H-atom concentration, both criteria giving results that differ typically by less than 5%, but the latter is inappropriate with the 5-step mechanism.

Reactant consumption and heat release can be neglected during the induction stage, so that the homogeneous-reactor problem reduces to that of integrating the evolution equations for the radicals

$$\frac{dC_H}{dt} = -k_1 C_{O_2} C_H + k_2 C_{H_2} C_O + k_3 C_{H_2} C_{OH} - k_4 C_{M4} C_{O_2} C_H + k_5 C_{O_2} C_{H_2} \tag{1}$$

$$\frac{dC_O}{dt} = k_1 C_{O_2} C_H - k_2 C_{H_2} C_O \tag{2}$$

$$\frac{dC_{OH}}{dt} = k_1 C_{O_2} C_H + k_2 C_{H_2} C_O - k_3 C_{H_2} C_{OH} \tag{3}$$

with initial conditions $C_H = C_O = C_{OH} = 0$, yielding a linear problem that has been considered in the past (see [15] and references therein). Here, C_i denotes the concentration of species i and C_{M4} is the effective third-body concentration of reaction 4, which accounts for the increased chaperon efficiency of H_2 according to $C_{M4} = (1 + 1.5X_{H_2})C_M$, where $C_M = p/(R^0 T)$ is the third-body concentration and $R^0 = 8.314$ J/(kg K) represents the universal gas constant. With reactant consumption neglected, the solution of the linear system (1)–(3) leads to unbounded radical growth, so that a criterion must be introduced to identify ignition conditions. For instance, one may identify ignition as the instant of time at which the H-atom concentration obtained from integration of (1)–(3) reaches a value equal to the initial H_2 concentration. In view of Fig. 1, since the peak radical concentration is somewhat smaller than the initial H_2 concentration, overpredictions on the order of 10% can be expected to be associated with this simple condition $C_H = C_{H_2}$.

2.2. The steady-state assumptions for O and OH

The problem can be simplified by exploiting the fact that the rate constants for reactions 2 and 3 are larger than that of reaction 1, so that for instance $k_1/k_2 = 0.318$ and $k_1/k_3 = 0.0746$ at $T = 1200$ K, thereby promoting rapid consumption of O and OH. The development begins by combining linearly (1)–(3) to eliminate the terms involving the fast reactions 2 and 3, yielding

$$\frac{d}{dt}(C_H + 2C_O + C_{OH}) = (2k_1 - k_4 C_{M4}) C_{O_2} C_H + k_5 C_{O_2} C_{H_2} \tag{4}$$

where a characteristic branching time

$$\tilde{t}_B = \frac{1}{(2k_1 - k_4 C_{M4}) C_{O_2}} \tag{5}$$

appears, and a characteristic initiation time

$$t_{\mathrm{I}} = \frac{1}{k_5 C_{\mathrm{O}_2}} \tag{6}$$

occurs, such that $\tilde{t}_{\mathrm{B}}/t_{\mathrm{I}} \sim k_5/k_1 \ll 1$. As can be seen in (4), an exponential radical growth takes place if the condition $2k_1 > k_4 C_{\mathrm{M4}}$ is satisfied, which occurs as long as the temperature is above a crossover temperature, defined for ignition by the equation

$$2k_1 = k_4(1 + 1.5X_{\mathrm{H}_2})p/\left(R^0 T\right) \tag{7}$$

giving for instance $T \simeq (930, 1250)$ K when evaluated at $p = (1, 20)$ atm with $X_{\mathrm{H}_2} = 0$. Note that a slightly different definition applies when the combustion conditions are such that the attack of HO_2 by radicals is nonnegligible, thereby modifying the effective radical growth rate, as occurs for instance in lean premixed flames [16,17].

An order-of-magnitude analysis serves to simplify the solution. Thus, with anticipated radical evolution times of order $\tilde{t}_{\mathrm{B}}$, the accumulation rates in (2) and (3) can be expected to be negligibly small when the conditions $k_2 C_{\mathrm{H}_2} \gg k_1 C_{\mathrm{O}_2}$ and $k_3 C_{\mathrm{H}_2} \gg k_1 C_{\mathrm{O}_2}$ are satisfied. If they are neglected, then (2) and (3) reduce to algebraic equations that can be solved to give the steady-state expressions

$$C_{\mathrm{O}} = \frac{k_1 C_{\mathrm{O}_2}}{k_2 C_{\mathrm{H}_2}} C_{\mathrm{H}} \tag{8}$$

and

$$C_{\mathrm{OH}} = \frac{2k_1 C_{\mathrm{O}_2}}{k_3 C_{\mathrm{H}_2}} C_{\mathrm{H}} \tag{9}$$

According to these two equations, in the limit $k_2 C_{\mathrm{H}_2} \gg k_1 C_{\mathrm{O}_2}$ and $k_3 C_{\mathrm{H}_2} \gg k_1 C_{\mathrm{O}_2}$ the concentrations of O and OH are much smaller than that of H. At leading order in the steady-state analysis, one may therefore neglect C_{O} and C_{OH} in (4) to yield

$$\frac{\mathrm{d}}{\mathrm{d}t}(C_{\mathrm{H}}) = (2k_1 - k_4 C_{\mathrm{M4}}) C_{\mathrm{O}_2} C_{\mathrm{H}} + k_5 C_{\mathrm{O}_2} C_{\mathrm{H}_2} \tag{10}$$

leading to

$$\frac{C_{\mathrm{H}}}{C_{\mathrm{H}_2}} = \frac{\tilde{t}_{\mathrm{B}}}{t_{\mathrm{I}}}\left(e^{t/\tilde{t}_{\mathrm{B}}} - 1\right) \tag{11}$$

upon integration with initial condition $C_{\mathrm{H}}(0) = 0$. The above expression indicates that for $t \sim \tilde{t}_{\mathrm{B}}$ the H-atom concentration reaches very small values of order $C_{\mathrm{H}} = (\tilde{t}_{\mathrm{B}}/t_{\mathrm{I}}) C_{\mathrm{H}_2}$. The results in Fig. 1 indicate that ignition is associated with radical concentrations becoming comparable to, although somewhat smaller than, the initial reactant concentrations, and therefore requires much larger times, which can be computed by using the ignition criterion $C_{\mathrm{H}} = C_{\mathrm{H}_2}$ in (11) to yield in the first approximation

$$t_{ig} = \tilde{t}_{\mathrm{B}} \ln\left(\frac{t_{\mathrm{I}}}{\tilde{t}_{\mathrm{B}}}\right) = \frac{1}{(2k_1 - k_4 C_{\mathrm{M4}}) C_{\mathrm{O}_2}} \ln\left(\frac{2k_1 - k_4 C_{\mathrm{M4}}}{k_5}\right) \tag{12}$$

for the ignition time, with $\ln(t_{\mathrm{I}}/\tilde{t}_{\mathrm{B}}) \sim 15$–$20$ for temperatures of practical interest.

The prediction given in (12) is compared in Fig. 2 with detailed-chemistry computations of ignition times using the temperature-inflection criterion. As can be seen, although the prediction is reasonably accurate for rich mixtures, giving overpredictions on the order of 10% that are consistent with the ignition criterion $C_{\mathrm{H}} = C_{\mathrm{H}_2}$ selected in deriving (12), increasing departures are found as the mixture becomes leaner, with (12) severely underpredicting the result. The reason for the identified failure is that the assumptions of fast O and OH consumption, used in deriving (10) from (4), rely on the conditions $k_2 C_{\mathrm{H}_2} \gg k_1 C_{\mathrm{O}_2}$ and $k_3 C_{\mathrm{H}_2} \gg k_1 C_{\mathrm{O}_2}$ and therefore become increasingly inaccurate as the fuel content decreases, resulting in significant underpredictions of ignition times for lean mixtures. In particular, while the detailed-chemistry computations predict ignition to be fastest near stoichiometric conditions, the steady-state expression (12) yields the minimum ignition time where the H_2 concentration vanishes. Hence, if utilized in mixing-layer computations, the steady-state assumptions for O and OH would lead to inaccurate predictions of ignition events, occurring too early and too far on the air side.

2.3. The radical-pool variable as a first-order correction

These inaccuracies of the O and OH steady-state assumptions have been known for quite some time, with different remedies proposed depending on the specific application of interest [18,19]. Following ideas developed previously [13], a different approach is taken here, based on the introduction of the radical-pool concentration $C = C_{\mathrm{H}} + 2C_{\mathrm{O}} + C_{\mathrm{OH}}$ appearing

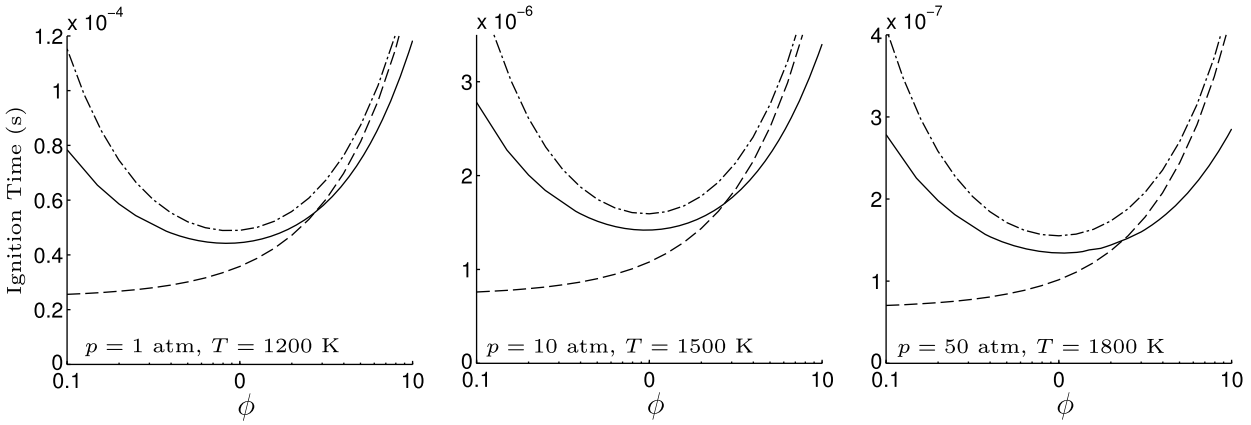

Fig. 2. The dependence on equivalence ratio ϕ of the ignition time of a hydrogen–air mixture as obtained in a homogeneous adiabatic reactor at constant pressure from numerical integrations with the SD mechanism using the temperature-inflection criterion (solid curves) and from evaluations of (12) (dashed curves) and of (17) (dot-dashed curves).

in the accumulation term of (4) for the description of the branched-chain explosion. The proposed strategy avoids the large inaccuracies associated with the neglect of the concentrations C_O and C_{OH}. In deriving an evolution equation for C, the steady-state expressions (8) and (9) are used to relate C with the H-atom concentration according to

$$C = C_H + 2C_O + C_{OH} = \left(1 + \frac{2k_1 C_{O_2}}{k_2 C_{H_2}} + \frac{2k_1 C_{O_2}}{k_3 C_{H_2}}\right) C_H \tag{13}$$

which is the employed to rewrite (4) in the form

$$\frac{dC}{dt} = \frac{(2k_1 - k_4 C_{M4}) C_{O_2} C_{H_2}}{C_{H_2} + 2(k_1/k_2 + k_1/k_3) C_{O_2}} C + k_5 C_{O_2} C_{H_2} \tag{14}$$

similar to (10) but involving a branching time

$$t_B = \frac{C_{H_2} + 2(k_1/k_2 + k_1/k_3) C_{O_2}}{(2k_1 - k_4 C_{M4}) C_{O_2} C_{H_2}} \tag{15}$$

that depends on the H_2 concentration and shows a minimum value for a mixture composition close to stoichiometric conditions. Integrating (14) with initial condition $C(0) = 0$ gives

$$\frac{C}{C_{H_2}} = \frac{t_B}{t_I}\left(e^{t/t_B} - 1\right) \tag{16}$$

which can be employed, together with the ignition condition $C = C_{H_2}$, to derive the expression

$$t_{ig} = t_B \ln\left(\frac{t_I}{t_B}\right) \tag{17}$$

for the ignition time, with t_I and t_B given, respectively, in (6) and (15) in terms of the composition and temperature. This last equation is shown in Fig. 2 to give reasonably accurate predictions of ignition times over the whole range of compositions, with overpredictions that are of the order of 10% for the most reactive conditions, found near stoichiometry, as is consistent with the ignition criterion selected. Similar inaccuracies can be expected to arise when using the radical pool in analyzing mixing-layer ignition problems, as is done below.

3. Formulation of the mixing-layer problem

3.1. Conservation equations

Consider the temporal evolution of two stagnant spaces of H_2 and air that begin to mix and react at time $t = 0$, with the air occupying initially the semi-space $x > 0$. In the weakly reactive solution observed prior to ignition, the reactants mix without appreciable chemical reaction, giving a nearly self-similar evolution for the reactant and temperature profiles. To describe the ignition process, including the self-similar mixing occurring in the absence of chemical reaction, it is convenient to formulate the problem in terms of the dimensionless coordinate $\eta = x/(D'_\infty t)^{1/2}$, where D'_∞ represents the value of the H_2–air binary diffusion coefficient evaluated at the air-side temperature. Correspondingly, the transverse velocity v' and the diffusion velocity V'_i of each species i are scaled with $(D'_\infty/t)^{1/2}$, yielding the dimensionless variables $v = v'/(D'_\infty/t)^{1/2}$

and $V_i = V_i'/(D_\infty'/t)^{1/2}$. The temperature, density, and thermal conductivity are scaled with the properties on the air side to give the dimensionless variables $T = T'/T_\infty'$, $\rho = \rho'/\rho_\infty'$, and $\kappa = \kappa'/\kappa_{A_\infty}'$. The problem reduces to that of integrating

$$\frac{\partial \rho}{\partial t} + \frac{1}{t}\left[(\rho v)_\eta - \frac{1}{2}\eta\rho_\eta\right] = 0 \tag{18}$$

$$\rho\frac{\partial Y_i}{\partial t} + \frac{1}{t}\left[\rho\left(v - \frac{\eta}{2}\right)Y_{i_\eta} + (\rho Y_i V_i)_\eta\right] = \frac{M_i\omega_i}{\rho_\infty'} \tag{19}$$

$$\frac{1}{T}\frac{\partial T}{\partial t} + \frac{1}{t}\left[\frac{1}{T}\left(v - \frac{\eta}{2}\right)T_\eta - L(\kappa T_\eta)_\eta\right] = -\sum_i \frac{h_i\omega_i}{\rho_\infty' c_{p_\infty}' t_\infty} \tag{20}$$

with initial conditions at $t = 0$

$$\eta > 0: \quad Y_i - Y_{i_\infty} = T - 1 = 0 \tag{21}$$

$$\eta < 0: \quad Y_i - Y_{i_{-\infty}} = T - T_{-\infty} = 0 \tag{22}$$

and boundary conditions for $t > 0$ given by

$$\eta \to +\infty: \quad v = Y_i - Y_{i_\infty} = T - 1 = 0 \tag{23}$$

$$\eta \to -\infty: \quad Y_i - Y_{i_{-\infty}} = T - T_{-\infty} = 0 \tag{24}$$

including a condition of zero displacement $v = 0$ on the air side. The resulting ignition time is independent of this last choice, in that introduction of a different condition for the transverse velocity, such as zero displacement $v = 0$ on the hydrogen side $\eta \to -\infty$, would cause a shift in the transverse location of the different profiles, but would not modify the resulting ignition time.

In the formulation, the subscript η is used to indicate differentiation with respect to this variable and the subscripts ∞ and $-\infty$ are employed for the magnitudes on the air and hydrogen sides, respectively. Here, Y_i, M_i, ω_i, and h_i represent, respectively, the mass fraction, molecular mass, chemical production rate (mols per unit volume per unit time), and molar enthalpy of species i. Since all species except for H_2, nitrogen and oxygen appear in negligibly small concentrations, the mass fraction of air in the mixture is given in the first approximation by $(1 - Y_{H_2})$, so that the equation of state reduces to

$$\rho T = \frac{1}{(M_A/M_{H_2})Y_{H_2} + 1 - Y_{H_2}} \tag{25}$$

in terms of the air-to-hydrogen molecular-mass ratio $M_A/M_{H_2} \simeq 14.5$. In writing (20) the specific heat per mol of gas mixture is assumed to be constant and equal to that found on the air side, so that the product of the density times the specific heat per unit mass c_p' is proportional to the reciprocal of the temperature according to $(\rho' c_p')/(\rho_\infty' c_{p_\infty}') = 1/T$, an excellent approximation for H_2–air gas mixtures in the temperature range considered (900 K $< t <$ 1800 K). The thermal conductivity is a function of the composition and temperature, with the simple expression

$$\kappa = \frac{\kappa_{H_2\text{-}A}(M_A/M_{H_2})^{2/3}Y_{H_2} + 1 - Y_{H_2}}{(M_A/M_{H_2})^{2/3}Y_{H_2} + 1 - Y_{H_2}}T^\sigma \tag{26}$$

suggested by Rosner [20], used below in computations, with $\kappa_{H_2\text{-}A} = \kappa_{H_{2_\infty}}'/\kappa_{A_\infty}' \simeq 7$ denoting the hydrogen-to-air thermal conductivity ratio evaluated at the air-side temperature and with the value $\sigma = 0.7$ employed for the presumed power-law temperature dependence. The Lewis number $L = \kappa_{A_\infty}'/(\rho_\infty' c_{p_\infty}' D_\infty')$ appearing in (20) is taken to be $L = 0.3$ in the computations.

3.2. Chemically frozen mixing layer

In the absence of chemical reaction, the solution is self-similar when expressed in terms of the variable η. Since the molecules of nitrogen and oxygen are very similar, for describing diffusion they can be treated as a single species with average molecular mass M_A, so that the mixture is effectively binary. The composition is determined in terms of Y_{H_2}, with the oxygen mass fraction obtained simply from $Y_{O_2} = Y_{O_{2A}}(1 - Y_{H_2})$, with $Y_{O_{2A}} = 0.232$ representing the oxygen mass fraction in the air mixture. The diffusion velocity of hydrogen can be obtained by solving exactly the Stefan–Maxwell

equation for a binary mixture to give the Fickian law [1]

$$Y_{\mathrm{H}_2} V_{\mathrm{H}_2} = -T_f^{1+\sigma} (Y_{\mathrm{H}_{2\eta}} - 0.29 Y_{\mathrm{H}_2} T_{f_\eta}/T_f) \tag{27}$$

which includes thermal diffusion, with T_f denoting the chemically-frozen temperature distribution and -0.29 used for the Soret factor. The problem reduces to that of integrating

$$(\rho v)_\eta - \frac{1}{2}\eta\rho_\eta = 0 \tag{28}$$

$$\left[\rho T_f^{1+\sigma}\left(Y_{\mathrm{H}_{2\eta}} - 0.29\frac{Y_{\mathrm{H}_2}}{T_f}T_{f_\eta}\right)\right]_\eta + \rho\left(\frac{1}{2}\eta - v\right)Y_{\mathrm{H}_{2\eta}} = 0 \tag{29}$$

$$LT_f(\kappa T_{f_\eta})_\eta + \left(\frac{1}{2}\eta - v\right)T_{f_\eta} = 0 \tag{30}$$

supplemented with (25) and (26) written for $T = T_f$, with boundary conditions

$$\eta \to +\infty: \quad v = Y_{\mathrm{H}_2} = T_f - 1 = 0 \tag{31}$$

$$\eta \to -\infty: \quad Y_{\mathrm{H}_2} - 1 = T_f - T_{-\infty} = 0 \tag{32}$$

The solution requires in general numerical integration for the computation of ρ, v, Y_{H_2}, and T_f as a function of η for a given value of the hydrogen-to-air temperature ratio $T_{-\infty}$, the only free parameter in the problem. As shown in [21], an analytic solution arises for the quasi-isothermal case $T_{-\infty} - 1 \ll 1$, when $T_f - 1 \ll 1$ everywhere across the mixing layer, thereby reducing the equation of state (25) to

$$Y_{\mathrm{H}_2} = \frac{M_{\mathrm{H}_2}}{M_{\mathrm{A}} - M_{\mathrm{H}_2}}\left(\frac{1}{\rho} - 1\right) \tag{33}$$

Differentiating the above equation and substituting the result into (29) gives

$$\rho\left(\frac{\rho_\eta}{\rho}\right)_\eta + \left(\frac{1}{2}\eta - v\right)\rho_\eta = 0 \tag{34}$$

which further reduces to $\rho(v + \rho_\eta/\rho)_\eta = 0$ by addition of (28). Integrating with the boundary conditions as $\eta \to +\infty$ provides

$$v = -\rho_\eta/\rho \tag{35}$$

which can be used in (28) to give the linear equation

$$\rho_{\eta\eta} + \frac{1}{2}\eta\rho_\eta = 0 \tag{36}$$

finally yielding

$$\rho = 1 - \frac{M_{\mathrm{A}} - M_{\mathrm{H}_2}}{2M_{\mathrm{A}}}\,\mathrm{erfc}\left(\frac{\eta}{2}\right) \tag{37}$$

upon integration, with erfc representing the complementary error function. This last expression can be used in (33) and (35) to determine the variation of Y_{H_2} and v across the mixing layer, along with the accompanying H_2 and O_2 mole fractions

$$X_{\mathrm{H}_2} = 1 - \frac{X_{\mathrm{O}_2}}{X_{\mathrm{O}_{2\,\mathrm{A}}}} = \frac{Y_{\mathrm{H}_2}}{Y_{\mathrm{H}_2} + (M_{\mathrm{H}_2}/M_{\mathrm{A}})(1 - Y_{\mathrm{H}_2})} \tag{38}$$

which can be seen to simplify to

$$X_{\mathrm{H}_2} = 1 - \frac{X_{\mathrm{O}_2}}{X_{\mathrm{O}_{2\,\mathrm{A}}}} = \frac{1}{2}\,\mathrm{erfc}\left(\frac{\eta}{2}\right) \tag{39}$$

3.3. Radical-pool conservation equation

Guided by the previous homogeneous-ignition results, to describe the chain-branching explosion in the mixing layer we introduce a radical-pool variable, so that the problem reduces to the integration of a single parabolic partial differential equation. As before, we begin by writing the conservation equations for the radicals H, O, and OH, obtained by writing (19) for the short chemistry description considered here to give

$$\frac{\partial Y_{\mathrm{H}}}{\partial t}+\frac{1}{t}\left[\left(\nu-\frac{\eta}{2}\right)Y_{\mathrm{H}_\eta}-\frac{1}{\rho}(\rho D_{\mathrm{H}}Y_{\mathrm{H}_\eta})_\eta\right]=\frac{M_{\mathrm{H}}}{\rho'}(-\omega_1+\omega_2+\omega_3-\omega_4+\omega_5)$$
$$\frac{\partial Y_{\mathrm{O}}}{\partial t}+\frac{1}{t}\left[\left(\nu-\frac{\eta}{2}\right)Y_{\mathrm{O}_\eta}-\frac{1}{\rho}(\rho D_{\mathrm{O}}Y_{\mathrm{O}_\eta})_\eta\right]=\frac{M_{\mathrm{O}}}{\rho'}(\omega_1-\omega_2)$$
$$\frac{\partial Y_{\mathrm{OH}}}{\partial t}+\frac{1}{t}\left[\left(\nu-\frac{\eta}{2}\right)Y_{\mathrm{OH}_\eta}-\frac{1}{\rho}(\rho D_{\mathrm{OH}}Y_{\mathrm{OH}_\eta})_\eta\right]=\frac{M_{\mathrm{OH}}}{\rho'}(\omega_1+\omega_2-\omega_3)$$

where a Fickian description is assumed for radical diffusion into the mixture, with D_i denoting the diffusivity of species i scaled with D'_∞. We proceed by combining the above equations to eliminate the singular rates ω_2 and ω_3, as done earlier in deriving (4), with the appropriate radical-pool variable being in this case

$$Y=Y_{\mathrm{H}}+2\frac{M_{\mathrm{H}}}{M_{\mathrm{O}}}Y_{\mathrm{O}}+\frac{M_{\mathrm{H}}}{M_{\mathrm{OH}}}Y_{\mathrm{OH}} \tag{40}$$

to be expressed as

$$Y=\left(1+\frac{2k_1X_{\mathrm{O}_2}}{k_2X_{\mathrm{H}_2}}+\frac{2k_1X_{\mathrm{O}_2}}{k_3X_{\mathrm{H}_2}}\right)Y_{\mathrm{H}} \tag{41}$$

with use made of the steady-state expressions (8) and (9) together with the identities $C_i=\rho Y_i/M_i=X_iC_{\mathrm{M}}$. The development is simplified if we assume constant values of D_i, because in the resulting linear combination the diffusive term can be expressed in terms of Y by introducing an effective diffusivity

$$D=\frac{D_{\mathrm{H}}+2(D_{\mathrm{O}}k_1/k_2+D_{\mathrm{OH}}k_1/k_3)X_{\mathrm{O}_2}/X_{\mathrm{H}_2}}{1+2(k_1/k_2+k_1/k_3)X_{\mathrm{O}_2}/X_{\mathrm{H}_2}} \tag{42}$$

thereby yielding the evolution problem

$$\frac{\partial Y}{\partial t}+\frac{1}{t}\left[\left(\nu-\frac{\eta}{2}\right)Y_\eta-\frac{1}{\rho}\left[\rho(DY)_\eta\right]_\eta\right]=\frac{Y}{t_{\mathrm{B}}}+\frac{X_{\mathrm{H}_2}M_{\mathrm{H}}/M}{t_{\mathrm{I}}} \tag{43}$$

subject to the initial and boundary conditions

$$\begin{aligned}&t=0\text{:}\quad Y=0\quad\text{for } -\infty<\eta<+\infty\\&t>0\text{:}\quad Y=0\quad\text{as } \eta\to\pm\infty\end{aligned} \tag{44}$$

Here, M is the mean molecular weight of the gas mixture. As in (14), the chemical times t_{I} and t_{B} are those defined in (6) and (15), which are functions of η to be calculated across the mixing layer from the chemically-frozen profiles T_f, X_{H_2}, and X_{O_2}.

Transverse diffusion of radicals will be seen to have a dominant effect on the mixing-layer evolution. This can be anticipated by considering the simplified description

$$\frac{Y}{X_{\mathrm{H}_2}M_{\mathrm{H}}/M}=\frac{t_{\mathrm{B}}}{t_{\mathrm{I}}}\left(e^{t/t_{\mathrm{B}}}-1\right) \tag{45}$$

obtained from (43) by neglecting the transport terms, i.e., the terms in square brackets. As can be seen, in the absence of radical transport, the radical pool at each transverse location would follow the exponential increase (16) of the homogeneous explosion, with a branching rate corresponding to the local conditions of composition and temperature, giving a maximum growth rate at the intermediate location $\eta=\eta^*$ where t_{B} is minimum. Since ignition requires values of $t/t_{\mathrm{B}}\sim\ln(t_{\mathrm{I}}/t_{\mathrm{B}})\gg 1$, the solution given by (45) would develop a pronounced peak at $\eta=\eta^*$, thereby promoting diffusive radical loss to the sides and reducing the peak growth rate. The predominant role of radical diffusion can be further appreciated by substituting (45) into (43), because the transport terms evaluated in that way turn out to be a factor t/t_{B} larger than the accumulation or branching terms. As shown below, to determine the ignition solution for times much larger than t_{B} full consideration must be given to the interplay between chemical production, local accumulation, and transverse transport of radicals.

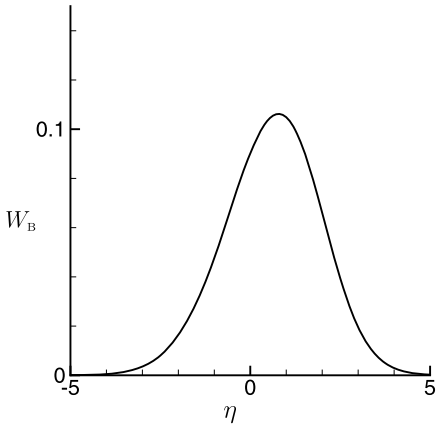

Fig. 3. The reduced branching rate W_B for the isothermal mixing layer evaluated from (48) for $k_1/k_2 = 0.318$ and $k_1/k_3 = 0.746$.

4. Asymptotic analysis

4.1. The WKB method

For the analysis it is convenient to use a dimensionless time $\tau = (2k_{1\infty} - k_{4\infty}C_{M\infty})C_{M\infty}t$ in writing the evolution equation (43) in the form

$$\frac{\partial Y}{\partial \tau} + \frac{1}{\tau}\left[\left(\nu - \frac{\eta}{2}\right)Y_\eta - \frac{1}{\rho}\left[\rho(DY)_\eta\right]_\eta\right] = W_B(\eta)Y + \varepsilon X_{O_2}X_{H_2} \tag{46}$$

The dimensionless branching rate $W_B(\eta) = [(2k_{1\infty} - k_{4\infty}C_{M\infty})C_{M\infty}t_B]^{-1}$ and the initiation-to-branching rate-constant ratio

$$\varepsilon = \frac{M_H}{M}\frac{k_5}{2k_{1\infty} - k_{4\infty}C_{M\infty}} \tag{47}$$

are to be computed from the reactant and temperature frozen distributions. For instance, for the isothermal mixing layer

$$W_B(\eta) = \frac{X_{O_2}X_{H_2}}{X_{H_2} + 2(k_1/k_2 + k_1/k_3)X_{O_2}} \tag{48}$$

with X_{H_2} and X_{O_2} given in (39), resulting in the branching-rate distribution shown in Fig. 3 for the values $k_1/k_2 = 0.318$ and $k_1/k_3 = 0.746$ associated with a temperature of 1200 K. This branching rate shows a maximum value $W_B^* \simeq 0.106$ at $\eta = \eta^* \simeq 0.787$, corresponding to the minimum of the branching time (15).

Since the value of ε is always small, the effect of initiation is only important for $t \sim t_B$, i.e., $\tau \sim O(1)$, when the value of Y is of order ε, and it is negligible for larger times. Ignition occurs when Y reaches values of order unity, which occurs for $t/t_B \sim \ln(t_I/t_B)$, corresponding in the present formulation to $\tau \sim \ln(\varepsilon^{-1}) \gg 1$. In analyzing ignition, one may therefore neglect the initial stage in which initiation is important and focus on the long-time evolution for $\tau \gg 1$ with initiation neglected in (46) and the radical pool taking the form

$$Y/\varepsilon = \exp\left[G_0(\eta)\tau + G_1(\eta)\tau^{1/2} + G_2(\eta) + \cdots\right] \tag{49}$$

Introducing the above expansion into (46) and solving sequentially the problems that arise at different orders in powers of τ determines the functions $G_0, G_1, G_2, \ldots$ as shown below.

4.2. The asymptotic development

Diffusion dominates the solution at leading order to yield $(G_{0_\eta})^2 = 0$, which can be integrated to give a constant value

$$G_{0_\eta} = G_0^* \tag{50}$$

revealing that, because of radical diffusion, the growth rate is uniform at leading order all across the mixing layer. The next nontrivial equation in the asymptotic development follows from the balance

$$G_0^* - DG_{1_\eta}^2 = W_B \tag{51}$$

between accumulation, diffusion and branching, which can be solved to give

$$G_{1_\eta} = \pm\sqrt{\frac{G_0^* - W_\mathrm{B}}{D}} \tag{52}$$

This equation indicates that G_0^* must be equal to the maximum branching rate $G_0^* = W_\mathrm{B}^*$, because if G_0^* were larger than W_B^*, then (52) would include a monotonically increasing solution and a monotonically decreasing solution, neither of them being valid, since they would lead to a radical-pool distribution diverging on one side of the mixing layer or on the other, and if G_0^* were smaller than W_B^*, then there would exist a central region where $G_0^* < W_\mathrm{B}$, giving imaginary values of G_1, corresponding to unrealistic oscillatory radical profiles.

The solution for G_1 follows from integrating (52) with $G_0^* = W_\mathrm{B}^*$ to give

$$G_1 = G_1^* + \begin{cases} -\int_{\eta^*}^{\eta} \frac{(W_\mathrm{B}^* - W_\mathrm{B})^{1/2}}{D^{1/2}}\,\mathrm{d}\eta & \text{for } \eta > \eta^* \\ +\int_{\eta^*}^{\eta} \frac{(W_\mathrm{B}^* - W_\mathrm{B})^{1/2}}{D^{1/2}}\,\mathrm{d}\eta & \text{for } \eta < \eta^* \end{cases} \tag{53}$$

where the minus and plus branches are selected for $\eta > \eta^*$ and for $\eta < \eta^*$ to ensure a nondiverging behavior. The peak value $G_1 = G_1^*$ is obtained from the equation at the following order, which can be cast in the form

$$2DG_{2_\eta} = \nu - \frac{\eta}{2} - \frac{(\rho D)_\eta}{\rho} - D_\eta + \frac{G_1/2 - DG_{1_{\eta\eta}}}{G_{1_\eta}} \tag{54}$$

As can be seen, to avoid the appearance of a singularity in the function G_{2_η} at $\eta = \eta^*$, where $G_{1_\eta} = 0$, the numerator in the last term must vanish at that location, thereby giving

$$G_1^* = 2D^* G_{1_{\eta\eta}}^* = -\left(-2D^* W_{\mathrm{B}_{\eta\eta}}^*\right)^{1/2} \tag{55}$$

with the value of $G_{1_{\eta\eta}}^* = -[W_{\mathrm{B}_{\eta\eta}}^*/(2D^*)]^{1/2}$ evaluated from higher-order derivatives of (51) at $\eta = \eta^*$.

At the order resolved here the development gives

$$Y/\varepsilon = \exp\left[W_\mathrm{B}^*\tau - \left(-2D^* W_{\mathrm{B}_{\eta\eta}}^*\right)^{1/2}\tau^{1/2}\right] \times \exp\left[\pm\int_{\eta^*}^{\eta} \frac{(W_\mathrm{B}^* - W_\mathrm{B})^{1/2}}{D^{1/2}}\,\mathrm{d}\eta\right] \tag{56}$$

for the radical-pool distribution. The peak in the radical pool

$$Y_\mathrm{max} = \varepsilon \exp\left[W_\mathrm{B}^*\tau - \left(-2D^* W_{\mathrm{B}_{\eta\eta}}^*\right)^{1/2}\tau^{1/2}\right] \tag{57}$$

is achieved at $\eta = \eta^*$. Radical growth is uniform at leading order, with a branching rate equal to its peak value at $\eta = \eta^*$. The first-order correction, associated with diffusive radical loss, involves the square root of the radical diffusivity times the curvature of the branching-rate distribution evaluated at $\eta = \eta^*$.

4.3. Results from the asymptotics

The results of the asymptotic analysis are compared in Fig. 4 with results of numerical integrations of (46) for the isothermal mixing layer. The leading-order prediction for the peak radical mass fraction

$$Y_\mathrm{max} = \varepsilon \exp\left(W_\mathrm{B}^*\tau\right) \tag{58}$$

and the corrected expression (57) are compared in left-hand-side plot with the numerical results. As expected, the solution (58) corresponding to radicals growing with the maximum branching rate tends to overpredict the radical-pool concentration. Accounting for diffusive radical loss improves significantly the accuracy of the results, giving a variation of Y_max with τ that is virtually indistinguishable from that obtained numerically for $\tau \gtrsim 30$ when plotted in logarithmic scale.

The full radical profiles are shown in the right-hand-side plot for different times. Reasonably good agreement is found between the numerics and the analytical results, the most noticeable difference being the transverse location of the radical peak Y_max. Thus, the asymptotic analysis for large times predicts Y_max to be at $\eta = \eta^*$, with $\eta^* \simeq 0.787$ for the isothermal case considered in the plot, whereas the numerical results give a peak in radical mass fraction closer to the fuel side. These departures can be explained by noting that radical growth is initially controlled by the initiation reactions, with a rate $\varepsilon X_{\mathrm{O}_2} X_{\mathrm{H}_2}$ in (46) that shows a maximum at $\eta = 0$ for the isothermal case. One may therefore expect radicals to initially peak near the center of the mixing layer. This is observed in the profiles of Fig. 4, where the radical peak progressively moves towards the air side as branching takes over for larger times, thereby approaching the asymptotic prediction.

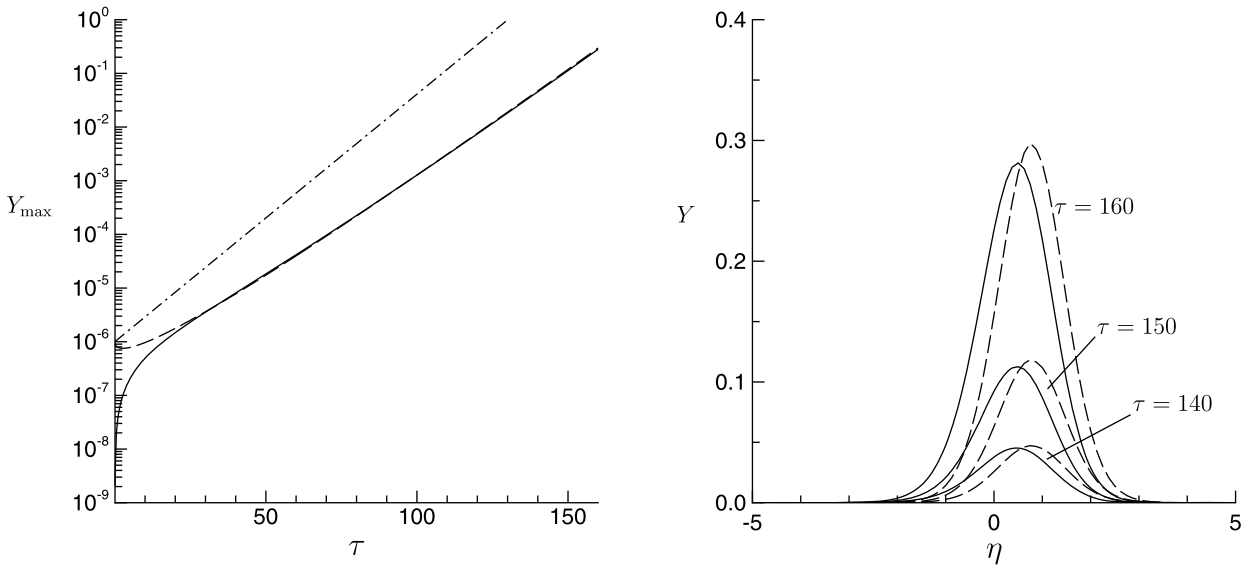

Fig. 4. The left-hand-side plot shows the evolution with time of the peak value of Y as obtained from numerical integration of (46) for $T_{-\infty} = 1$, $D = 1$, and $\varepsilon = 10^{-6}$ (solid lines), from the leading-order prediction $Y_{\max} = \varepsilon \exp[W_{\mathrm{B}}^{*}\tau]$ (dot-dashed curves), and from the first-order correction $Y_{\max} = \varepsilon \exp[W_{\mathrm{B}}^{*}\tau - (-2D^{*}W_{\mathrm{B}_{\eta\eta}}^{*})^{1/2}\tau^{1/2}]$ (dashed curves). The right-hand-side plot compares the corresponding radical-pool profiles determined numerically (solid lines) with the asymptotic prediction (56) (dashed curves).

4.4. Ignition time and ignition distance

Although including higher-order terms in (49) would increase the accuracy of the asymptotic development, the order of the expansion considered here provides sufficient accuracy for most purposes. Predictions of ignition times follow from using the ignition criterion $Y = X_{\mathrm{H}_2}^{*} M_{\mathrm{H}}/M$, equivalent to the criterion $C = C_{\mathrm{H}_2}$ employed in deriving (17), together with the asymptotic predictions for the peak radical mass fraction given in (57) and (58). At leading order, the simple expression

$$t_{ig} = t_{\mathrm{B}}^{*} \ln\left[t_{\mathrm{I}}^{*}/t_{\mathrm{B}}^{*}\right] \tag{59}$$

is obtained from (58) when small relative errors of order $\ln(\varepsilon^{-1})$ are neglected to write the term in the logarithm in compact form. Here, t_{B}^{*} is the minimum of the branching time across the mixing layer, which can be computed from (15) from the chemically frozen profiles of temperature and of oxygen and hydrogen mole fractions, and t_{I}^{*} is the corresponding initiation time, evaluated from (6) at $\eta = \eta^{*}$.

The mixing-layer analysis presented here can be applied in an approximate way to obtain estimates of autoignition distances l_{ig} in practical nonpremixed combustion devices by multiplying the ignition time (59) by an appropriately selected average velocity. This simple approach, neglecting the effect of flow strain on the mixing and reaction in the mixing layer, provides reasonable results. As an illustrative example, we consider the experiment of [10], including a hydrogen jet with velocity 1780 m/s and temperature $T'_{-\infty} = 545$ K and a hot co-flow of vitiated air with oxygen mass fraction $X_{\mathrm{O}_2\mathrm{A}} = 0.201$ at velocity 1420 m/s and temperature $T'_{\infty} = 1250$ K. The self-similar profiles T_f and $X_{\mathrm{H}_2} = 1 - X_{\mathrm{O}_2}/X_{\mathrm{O}_2\mathrm{A}}$, obtained from integrating (28)–(30), can be used in (15) to obtain the values $\eta^{*} = 1.347$ and $t_{\mathrm{B}}^{*} = 2.5 \times 10^{-6}$ s, and in (6) to give $t_{\mathrm{I}}^{*} = 26.73$ s. Substituting these two values in (59) then yields $t_{ig} = 4.05 \times 10^{-5}$ s that, when multiplied by an average convective velocity of 1600 m/s, finally gives $l_{ig} = 6.47$ cm for the ignition distance, very close to the value $l_{ig} = 5.9$ cm reported in the experiment.

5. Concluding remarks

We have addressed here branched-chain explosions in mixing layers, which determine the lift-off distance of hydrogen–air diffusion flames in high-speed combustion devices, such as SCRAMJETS. The development includes the derivation, based on the disparity of chemical time scales, of an evolution equation for the radical pool that effectively corrects departures of steady-state assumptions previously identified. The disparity of chemical times is also used in obtaining an analytical solution for the chain-branching explosion. It is seen that radical diffusion causes radical growth to proceed at a uniform rate at leading order all across the mixing layer, with a value associated with the minimum branching time t_{B}^{*}, found at an intermediate location. Radical loss by diffusion enters at the following order to determine the shape of the radical profiles and correct the resulting peak value.

Of interest for practical applications is the predictions of ignition times that may be derived from the analysis, including the simple expression (59). Assuming the mixing-layer element to be convected with a mean velocity, intermediate between

those of the two feed streams, results in predictions of ignition distances that compare well with previous experimental results. The agreement found is illustrative of how simple analytical methods not only serve to clarify the effect of the competing physicochemical phenomena but also produce quantitative results of practical applicability when the computation includes an accurate account of density and transport properties, as done here when evaluating the controlling chemical times t_B^* and t_I^*. The resulting demonstrated applicability of a highly simplified, but properly developed model to real-world turbulent-combustion situations seems truly remarkable.

Acknowledgements

We thank Paul Clavin for years of fruitful scientific discussions. In particular, the work presented here was motivated by the insightful questions he posed during the PhD defense of P.B. [9]. This work was supported by US AFOSR Grant #FA9550-12-1-0138.

References

[1] F.A. Williams, Combustion Theory, 2nd ed., Benjamin Cummings, Menlo Park, CA, 1985.
[2] A. Liñán, Ignition and flame spread in laminar mixing layers, in: J. Buckmaster, T.L. Jackson, A. Kumar (Eds.), Combustion in High-Speed Flows, Kluwer Academic Publ., 1994, pp. 461–476.
[3] T. Niioka, Ignition time in the stretched flow field, Proc. Combust. Inst. 18 (1981) 1807–1813.
[4] E. Mastorakos, Ignition of turbulent non-premixed flames, Progr. Energy Combust. Sci. 35 (2009) 57–97.
[5] A. Liñán, A. Crespo, An asymptotic analysis of unsteady diffusion flames for large activation energies, Combust. Sci. Technol. 14 (1976) 95–117.
[6] B. Lewis, G. Von Elbe, Combustion, Flames and Explosions in Gases, Pergamon Press, New York, 1951.
[7] P. Boivin, A.L. Sánchez, F.A. Williams, Explicit analytic prediction for hydrogen–oxygen ignition times at temperatures below crossover, Combust. Flame 159 (2012) 748–752.
[8] P. Boivin, A. Dauptain, C. Jimenez, B. Cuenot, Simulation of a supersonic hydrogen–air autoignition-stabilized flame using reduced chemistry, Combust. Flame 159 (2012) 1779–1790.
[9] P. Boivin, Reduced-kinetic mechanisms for hydrogen and syngas combustion including autoignition, PhD thesis, Universidad Carlos III de Madrid, 2011.
[10] T.S. Cheng, J.A. Wehrmeyer, R.W. Pitz, O. Jarret Jr., G.B. Northam, Raman measurement of mixing and finite-rate chemistry in a supersonic hydrogen–air diffusion flame, Combust. Flame 99 (1994) 157–173.
[11] A.L. Sánchez, A. Liñán, F.A. Williams, A WKB analysis of radical growth in the hydrogen–air mixing layer, J. Engrg. Math. 31 (1997) 119–130.
[12] A.L. Sánchez, A. Liñán, F.A. Williams, Chain-branching explosions in mixing layers, SIAM J. Appl. Math. 59 (1999) 1335–1355.
[13] J.D. Mellado, A.L. Sánchez, J.S. Kim, A. Liñán, Branched-chain ignition in strained mixing layers, Combust. Theory Model. 4 (2000) 265–288.
[14] P. Saxena, F.A. Williams, Testing a small detailed chemical-kinetic mechanism for the combustion of hydrogen and carbon monoxide, Combust. Flame 145 (2006) 316–323, also available at http://maemail.ucsd.edu/combustion/cermech.
[15] G. del Álamo, F.A. Williams, A.L. Sánchez, Hydrogen–oxygen induction times above crossover temperatures, Combust. Sci. Technol. 176 (2004) 1599–1626.
[16] D. Fernández-Galisteo, A.L. Sánchez, A. Liñán, F.A. Williams, One-step reduced kinetics for lean hydrogen–air deflagration, Combust. Flame 156 (2009) 985–996.
[17] D. Fernández-Galisteo, A.L. Sánchez, A. Liñán, F.A. Williams, The hydrogen–air burning rate near the lean flammability limit, Combust. Theory Model. 13 (2009) 741–761.
[18] F. Mauss, N. Peters, B. Rogg, F.A. Williams, Reduced kinetic mechanisms for premixed hydrogen flames, in: N. Peters, B. Rogg (Eds.), Reduced Kinetic Mechanisms for Applications in Combustion Systems, Springer-Verlag, Heidelberg, 1993, pp. 29–43.
[19] P. Boivin, C. Jiménez, A.L. Sánchez, F.A. Williams, An explicit reduced mechanism for H_2–air combustion, Proc. Combust. Inst. 33 (2011) 517–523.
[20] D.E. Rosner, Transport Processes in Chemically Reacting Flows, Dover, 2000.
[21] A.L. Sánchez, M. Vera, A. Liñán, Exact solutions for transient mixing of two gases of different density, Phys. Fluids 18 (2006) 078102.